The Ag dielectric function in plasmonic metamaterials

Vladimir P. Drachev, Uday K. Chettiar, Alexander V. Kildishev, Hsiao-Kuan Yuan, Wenshan Cai, and Vladimir M. Shalaev

Birck Nanotechnology Center and School of Electrical and Computer Engineering, Purdue University, West Lafayette, IN 47907, USA
vdrachev@purdue.edu

Abstract: Ag permittivity (dielectric function) in coupled strips is different from bulk and has been studied for strips of various dimensions and surface roughness. Arrays of such paired strips exhibit the properties of metamagnetics. The surface roughness does not affect the Ag dielectric function, although it does increase the loss at the plasmon resonances of the coupled strips. The size effect in the imaginary part of the dielectric function is significant for both polarizations of light, parallel and perpendicular to the strips with relatively large A-parameter.

OCIS codes: (160.3918) Metamaterials; (160.3900) Metals; (260.5740) Resonance; (260.3910) Metal optics.

References and links

1. A. Kawabata and R. Kubo, "Electronic properties of fine metallic particles. II. Plasma resonance absorption," J. Phys. Soc. Jpn. **21**, 1765 (1966).
2. L. P. Gor'kov and G. M. Eliashberg, "Minute metallic particles in an electromagnetic field," Sov. Phys. JETP **21**, 940 (1965).
3. U. Kreibig and M. Vollmer, *Optical properties of metal clusters*, (Springer-Verlag: Berlin, Heidelberg, 1995).
4. H. Hövel, S. Fritz, A. Hilger, U. Kreibig, and M. Vollmer, "Width of cluster plasmon resonances: bulk dielectric functions and chemical interface damping," Phys. Rev. B **48**, 18178 (1993).
5. A. Hilger, M. Tenfelde and U. Kreibig, "Silver nanoparticles deposited on dielectric surfaces," Appl. Phys. B **73**, 361 (2001).
6. B. N. J. Persson, "Surface resistivity and vibrational damping in adsorbed layers," Phys. Rev. B **44**, 3277 (1991).
7. B. N. J. Persson, "Polarizability of small spherical metal particles: influence of the matrix environment," Surface Science **281**, 153 (1993).
8. K. Charlé, F. Frank, and W. Schulze, "The optical properties of silver microcrystallites in dependence on size and the influence of the matrix environment," Ber. Bunsenges. Phys. Chem. **88**, 350 (1984).
9. A. V. Pinchuk, U. Kreibig, and A. Hilger, "Optical properties of metallic nanoparticles: influence of interface effects and interband transitions," Surface Science **557**, 269 (2004).
10. H.-K. Yuan, U. K. Chettiar, W. Cai, A. V. Kildishev, A. Boltasseva, V. P. Drachev, and V. M. Shalaev, "A negative permeability material at red light," Opt. Express **15**, 1076 (2007).
11. W. Cai, U. K. Chettiar, H.-K. Yuan, V. C. de Silva, A. V. Kildishev, V. P. Drachev, and V. M. Shalaev, "Metamagnetics with rainbow colors," Opt. Express **15**, 3333 (2007).
12. P. B. Johnson and R. W. Christy, "Optical constants of the noble metals," Phys. Rev. B **6**, 4370 (1972).
13. D. W. Lynch and W. R. Hunter, in *Handbook of Optical Constants of Solids*, E. D. Palik, ed. (Academic Press: New York, 1985).
14. M. J. Weber, *Handbook of optical materials*, (CRC: New York, 2003).
15. W. A. Kraus and G. C. Schatz, "Plasmon resonance broadening in small metal particles," J. Chem. Phys. **79**, 6130 (1983).
16. *COMSOL Multiphysics. Command Reference*, Comsol AB: Stockholm, Sweden, 2007.

#90392 - $15.00 USD Received 3 Dec 2007; revised 10 Jan 2008; accepted 11 Jan 2008; published 16 Jan 2008

1. Introduction

Metal nanostructures support localized surface plasmons and propagating waves, known as surface plasmon-polaritons. The variety of applications of plasmonic nanostructures includes molecular sensing and imaging, all-optical devices, sub-wavelength waveguides and integrated circuits, and metamaterials with optical magnetism and negative refractive index. Advanced fabrication and computation methods allow the engineering of optimal nanostructure geometries of metal dielectric composites aimed at particular application. The fundamental properties of the metal and the artificially designed geometries of the structural units enable the needed functionality for the nanostructures. Thus, the dielectric function of metal is a key factor for the design and optimization of plasmonic nanostructures. However, the dielectric function of nanostructured metallic elements differs from ideal bulk metal [1-3] especially in the imaginary part. The difference depends on many factors, including the surrounding media and the dimensions and shapes of the elements. This is why the dielectric function of nanostructured metal has been under comprehensive study for many years [3]. Size effects are more significant as the dimensions become comparable to the electron mean free path, which is about 50 nm for silver [3]. The size-dependent contribution to the electron relaxation rate involves several mechanisms. Among them are the quantum size effect and the chemical interface effect caused by static and dynamic charge transfer between a particle and the surrounding material [4-9].

Previous studies of Ag dielectric functions in nanostructures were focused mostly on spherical nanoparticles or spheroids. Structures such as nanowires and nanostrips are less studied, although they are of great interest for nanoscale wave-guiding and metamaterial applications. Here we report on experiments involving paired nanostrips fabricated with e-beam lithography. Special, asymmetric plasmon modes in such coupled strips result in circular currents and consequently a magnetic response at the magnetic plasmon resonance. Paired strips arranged in a sub-wavelength grating can produce a material with an optical permeability other than unity. Negative permeability of the effective layer containing a grating of paired strips has been reported for the whole visible spectral range in our recent papers [10-11].

Nanofabrication with e-beam lithography allows one to control not only the dimensions of a metal-dielectric structure, but also the roughness of the metal-dielectric interface. Here we study the Ag dielectric function in strips with different roughness of the silver surface or different strip dimensions. Note that Ag has the lowest losses in the optical range. However, the literature provides very different data even for the bulk permittivity of Ag [12-14], especially in the imaginary part as illustrated in Fig. 1. The real parts of the dielectric function obtained from the different sources agree reasonably well with each other as is shown in Fig. 1(a). However, the imaginary parts show large discrepancies amongst the three sources (Fig. 1 (b),(c)). All these sources are equally used in the current literature as references for Ag permittivity. In our case the data from Johnson and Christy [12] gave the best agreement with experimental observations.

The dielectric function of a bulk noble metal at the frequency ω is well described by the Drude-Lorentz-Sommerfeld formula for the conduction electrons using an additional contribution from interband electron transitions between the valence and conduction bands:

$$\varepsilon_m(\omega) = 1 - \frac{\omega_p^2}{\omega(\omega + i\gamma_\infty)} + 4\pi\chi_{ib}, \tag{1}$$

where γ_∞ is the phenomenological relaxation constant of bulk metal, χ_{ib} is the interband term of the metal susceptibility, and $\omega_p = \sqrt{4\pi n e^2 / m_e}$ is the plasma frequency, with n, e, m_e being the density of free electrons, electron charge and effective electron mass, respectively.

In classical theory, damping in the dielectric function above is due to the collision of electrons with electrons, phonons, and lattice defects or grains boundaries; the total damping

#90392 - $15.00 USD Received 3 Dec 2007; revised 10 Jan 2008; accepted 11 Jan 2008; published 16 Jan 2008

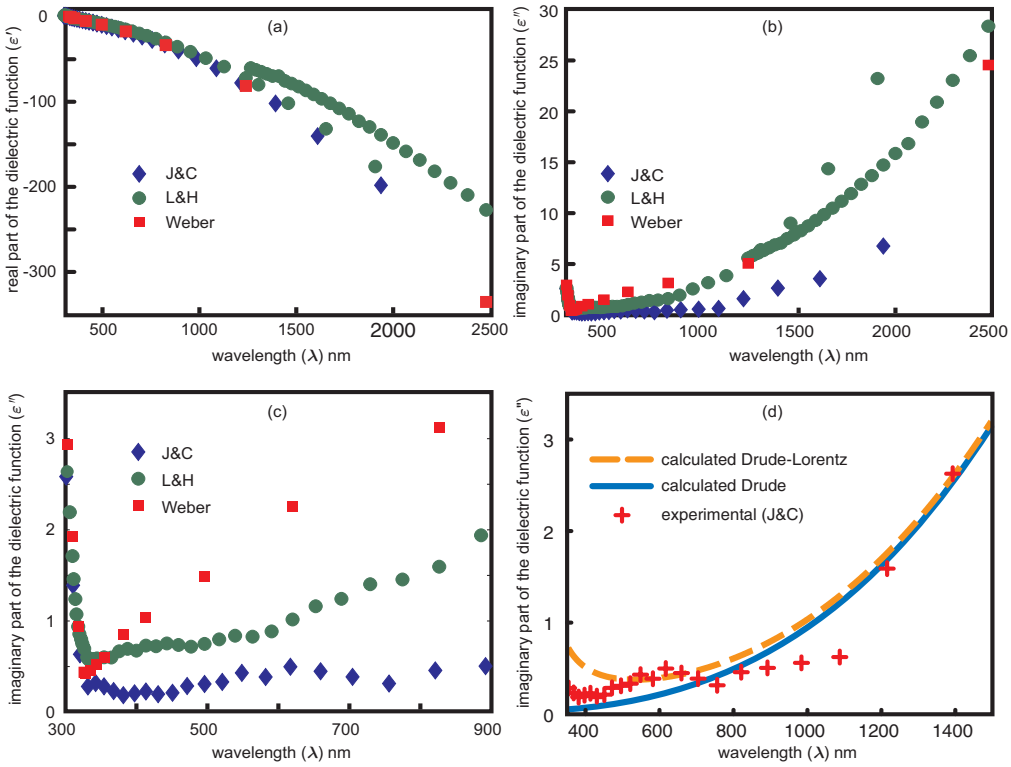

Fig. 1. (a) and (b): Real part and imaginary part of the dielectric function of bulk silver from various sources in the literature, J&C [12], L&H [13], and Weber [14]; (c) The same as (b) but only the visible range; (d) Imaginary part of the bulk Ag dielectric function: experiment Ref. [12] (red crosses), Drude-Lorentz approximation (dashed orange line), Drude term (blue solid line).

term is the sum of the individual rates, $\gamma_\infty = \nu_{ee} + \nu_{ep} + \nu_{ed}$. The collision rate of electrons with defects and grains boundaries, ν_{ed}, could be responsible for the diversity in the literature data for $\varepsilon_m''(\omega)$ of Ag. Note that the smallest $\varepsilon_m''(\omega)$ was obtained by Johnson and Christy for thin (about 34 nm) large-area films [12]. Those films were deposited at very fast deposition rates (50 Å/s), after which they were polished and annealed . In opposition to large-area films, we obtained smooth nanostructure surfaces at a very low deposition rates of about 0.5 Å/s, although different rates up to 80 Å/s were tested in our experiments.

The classical free-path-effect model implies interactions of the electrons with the particle surface that result in an additional, size-dependent term in the damping constant:

$$\gamma(R) = \gamma_\infty + AV_F/R, \tag{2}$$

where the A parameter, the coefficient of the Fermi velocity to particle radius ratio, includes details of the scattering process. As follows from the classical model, the particle surface roughness should increase the relaxation rate.

A significant source of the electron damping rate is the chemical interface effect. A direct comparison of the plasmon resonance width for free particles and that for particles embedded in a matrix allows one to extract the influence of the interface effect on the A parameter [4]. In the case of Ag particles in a matrix Al_2O_3, experiments give *A = 0.6* for the particles on a substrate and *A = 1.6* for fully imbedded particles in a matrix, in contrast to *A = 0.25* for spherical particles in vacuum [5]. This additional contribution of the chemical interface damping was first mentioned by Persson [6-7], as $A = A_{\text{size}} + A_{\text{interface}}$, to explain experimental findings by Charle with coauthors [8].

#90392 - $15.00 USD Received 3 Dec 2007; revised 10 Jan 2008; accepted 11 Jan 2008; published 16 Jan 2008

The quantum mechanical solution for a rectangular prism (the approximate shape of the strips) predicts anisotropy of the size-dependent term. The size-dependent contribution to the relaxation rate for a rectangular prism with the field applied along the x axis is [15]

$$\gamma_{size} = \frac{3}{2}\left(\frac{3}{\pi}\right)^{1/3}\frac{V_F}{L_x}. \tag{3}$$

This result suggests anisotropy of the dielectric function of the metal strips if the size effect is significant.

In this work the simulated transmission and reflection spectra of the samples are fitted with the experimental ones by incorporating an adjusted value of the bulk-metal permittivity of silver. Here we approximate the interband term in the spectral range of interest, about 380 to1000 nm, by a Lorentzian tail which gives the best fitting to the Johnson and Christy experiments [12], as shown in Fig. 1(d):

$$\varepsilon_m(\omega,\alpha,\beta) = 1 - \frac{\omega_p^2}{\omega(\omega - i\alpha\gamma_\infty)} + \frac{f\omega_L^2}{\omega_L^2 - \omega^2 + i\beta\Gamma_L\omega}, \tag{4}$$

where $\omega_p = 9.17\,\mathrm{eV}$, $\gamma_\infty = 0.021\,\mathrm{eV}$, $f = 2.2$, $\omega_L = 5.27\,\mathrm{eV}$, $\Gamma_L = 1.14\,\mathrm{eV}$, α and β are adjustable parameters, $\alpha = \beta = 1$ for bulk metal data from [12].

The measured transmission and reflection spectra of several samples are matched with those simulated by a frequency domain finite element method (FEM). The size-dependent term of ε_m'' is clearly identified with relatively large A-parameter. It follows from the above considerations that surface roughness could potentially affect the metal dielectric function and distort the nanostructure geometry. Surface roughness was introduced in the modeling of the paired strips. Surprisingly, the geometrical effect of roughness is mostly responsible for increased losses at the plasmon resonances of the nanostructure, while the surface roughness does not affect the Ag permittivity. Anisotropy in ε_m'' observed in the experiments indicates a significant contribution from the quantum size effect and the chemical interface effect.

Note that both size-dependent permittivity of Ag and surface roughness affect the effective parameters of metamaterials. Relative to prototypes simulated with the bulk-metal permittivity, larger surface roughness acts to significantly decrease the real part of effective permeability $|\mu'|$ at the resonances, as we will see from the data presented.

2. Experiment

Five grating samples with different nanostrip widths and roughness have been fabricated and studied. Initial test samples with different silver surface roughness values were fabricated by varying the silver deposition rate from 80 Å/s to 0.5 Å/s. Results for those samples showed that a lower deposition rate provided lower roughness. To further investigate the situation of relatively low roughness, for the experiments presented herein we deposited four samples with a rate of about 0.5 Å/s and one with 2 Å/s. A complete set of the parameters for all five samples is presented in Table 1. Among the samples there are three samples of similar widths but different roughness values (# 1-3), and three samples of different widths fabricated in the same session (# 3-5).

Figure 2(a) shows the sub-wavelength grating structure elementary cell cross-section, which reflects the fabrication procedure resulting in a trapezoidal shape of the stacked strips. The elementary cell consists of a pair of thin silver strips with thickness t and width w. The strips are separated by an alumina spacer of thickness d, width w, and a refractive index of $n = 1.62 + 0i$. The sub-wavelength lattice constant of the grating is p. In all the structures, the periodicity p was varied to preserve almost the same metal coverage. Due to the fabrication process, the top width w_t is smaller than the bottom width w_b. In addition, two thin 10-nm layers of alumina are added, one between the lower silver strip and the substrate, and the second on top of the structure. The top alumina layer preserves the silver layer during

#90392 - $15.00 USD Received 3 Dec 2007; revised 10 Jan 2008; accepted 11 Jan 2008; published 16 Jan 2008

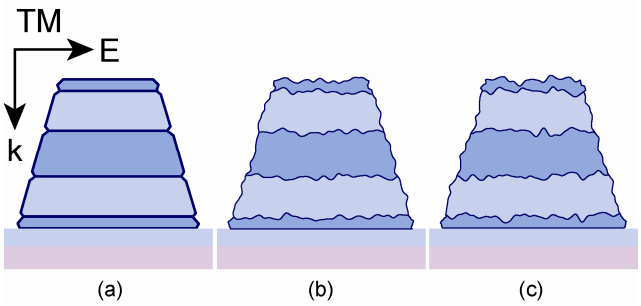

Fig. 2. Paired strips geometry with different roughness. (a) Ideal structure, $\delta = 0$, (b) $\delta = 1.5\,\mathrm{nm}$, and (c) $\delta = 2.0\,\mathrm{nm}$.

the lift-off process. As an example, Fig. 2(b),(c) shows the paired strips with modeled roughness.

Electron beam lithography techniques have been used to fabricate the samples. First, the geometry of the periodic strips was defined in resist by use of an electron beam writer (JEOL JBX-6000FS) on a glass substrate initially coated with a 15-nm film of indium-tin-oxide (ITO). Then, a stack of lamellar films was deposited with vacuum electron beam evaporation. Finally, a lift-off process was performed to obtain the desired silver strips.

The root-mean square (RMS) roughness measured within randomly selected areas on the top surface of the strips was determined with an atomic-force microscope (AFM, Veeco Dimension). A slower deposition rate of silver (0.5 Å/s, Samples 2-4) resulted in lower surface roughness than a faster deposition rate (~2Å/s, Sample 1). During our experiments we observed that the deposition rate cannot be set lower than 2 Å/s using a typical deposition procedure because the metal deposition heats the resist material too much and makes the lift-off process impossible. To cool down the resist, we performed an original multi-step deposition process with 10-minute pauses between each deposition step. This new procedure allows the use of a slower deposition rate of about 0.5 Å/s in order to obtain a lower surface

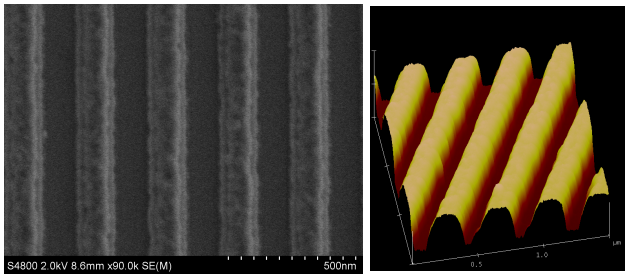

Fig. 3. Example of field emission scanning electron microscope and atomic force microscope images (sample #2).

roughness while ensuring successful lift-off, providing an overall better quality sample. The parameters of the fabricated samples are collected in Table 1, which includes dimensions of all the samples and characterization results. A representative field-emission scanning electron microscope (FE SEM) and AFM image of an example case (sample #2) are shown in Figs. 3(a) and 3(b).

2D surface roughness at the boundaries of silver strips is simulated by random displacements taken at discrete sets of surface points. The points of a given set are equidistantly distributed along the closed boundary defined by the ideal cross-section of a corresponding metallic strip. The distance between the points, ξ , gives to the correlation length of the roughness. Lengths from about 3-nm to 9-nm have been preliminary tested; of those, a correlation length of about 7 nm gives the best agreement with experimental results.

#90392 - $15.00 USD Received 3 Dec 2007; revised 10 Jan 2008; accepted 11 Jan 2008; published 16 Jan 2008

The final correlation length for each set is slightly adjusted to provide an even number of points along a given cross-section boundary. The local surface displacements are simulated using finite sets of random numbers (δ_p , $p = 0,1\ldots p_{\max}$) with the uniform distribution between -0.5 and 0.5 . Each set is scaled to provide roughness with a required root mean square (RMS) value, $\delta = s\sqrt{\sum \delta_p^2}\Big/p_{\max}$, where s is an individual scaling factor and $p_{\max}$ is the total number of points in a given set. Each p^{th} point is then displaced at a distance of $s\delta_p$ perpendicular to the initially ideal boundary. A 2D generating line of a given rough surface is then arranged as a smooth closed curve that passes through the displaced points. Each curve is created automatically through an intrinsic spline-interpolation procedure and is guaranteed to have continuous second derivatives [16]. The simulations are carried out using finite element method with 5^{th}-order elements and adaptive meshing. The smooth spline-interpolated boundaries are essential for reducing topological difficulties of adaptive meshing. Nonetheless, a few bad realizations are still very occasionally giving topologically degenerate mesh cases; such boundaries are replaced by topologically better realizations with the same RMS and correlation length. For each value of δ , 20 valid random realizations are simulated to obtain statistically representative data. Figure 2 depicts the selected examples of roughness realizations with $\delta = 1.5\,\text{nm}$ (Fig. 2(b)), and $\delta = 2\,\text{nm}$ (Fig. 2(c)); a corresponding ideal structure is shown in Fig. 2(a).

The transmission and reflection spectra of the samples were measured at normal incidence with a spectroscopy system appropriate for small area (160x160 μm) samples. The system contains an ultra-stable tungsten lamp (B&W TEK BPS100), a Glan Taylor prism polarizer, a spectroscopic collection device (SpectraCode), a spectrograph (Acton SpectraPro 300i), and a liquid-nitrogen cooled CCD-detector (Roper Scientific). The transmission and reflection spectra were normalized to a bare substrate and a calibrated silver mirror, respectively. To test that the collection area is less than the sample area the reflection spectra were first collected from a calibrated aperture in a highly reflective foil (Tedd Pella). The reflected signal was typically less than 1%. Reflection and transmission spectra were collected for both the TM and TE polarizations of incident light. In the resonant (TM) polarization, the magnetic field is aligned with the largest dimension of the structure – the infinite length of the strips. Only one component of the magnetic field should ideally be present in this case. In the non-resonant (TE) polarization, the single component of the electric field is aligned with the strip length, giving no resonant effects.

3. Results and discussion

One can see in spectra shown in Fig. 4(a,b) that the nanostrip structures exhibit both magnetic (asymmetric plasmon mode) and electric resonances under TM illumination (see Fig. 2 for polarization definitions). For the TE polarization, the structure has no resonant effects. In this case the samples act simply as diluted metals with behavior similar to perfect metals (Fig. 4(d)): more reflection and less transmission at longer wavelengths. Fig. 4 also shows spectra for an effective optical density defined as $D = \log(1-R) - \log T$. Such a definition accounts for light transmittance relative to the nonreflected portion. These spectra of the effective optical density emphasize the absorptive features of the nanostructures. The notion of D is found to be useful for fitting the simulated spectra with variable imaginary part of dielectric function. The short wavelength resonance in the optical spectra corresponds to the electric plasmon resonance, and the corresponding magnetic plasmon resonance relates to the long wavelength resonance. The effective parameter retrieval procedure is described in our previous papers [10-11].

#90392 - $15.00 USD Received 3 Dec 2007; revised 10 Jan 2008; accepted 11 Jan 2008; published 16 Jan 2008

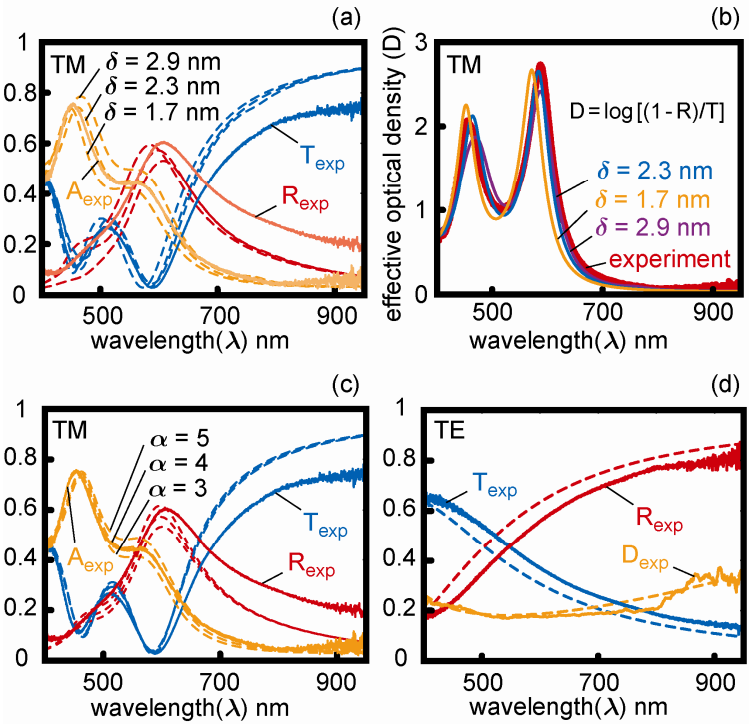

Fig. 4. TM polarization spectra (a)-(c): (a) simulated (dashed lines) spectra of transmission (blue), reflection (red), and absorption (orange) for one of the samples (sample #4) calculated with different the RMS surface roughness vs. the experimental data (solid lines); (b) simulated effective optical density D obtained for the RMS surface roughness (orange, $\delta = 1.7$ nm, purple, $\delta = 2.3$ nm, and blue, $\delta = 2.9$ nm) vs. the experimental data (red). (c) simulated effective optical density D obtained for the RMS surface roughness (orange, $\delta = 1.7$, blue, $\delta = 2.3$, and purple, $\delta = 2.9$). TE polarization spectra (d): experimental (solid lines) and simulated (dashed lines) spectra of transmission (blue), reflection (red), and effective optical density (orange).

Figure 4 (a-c) illustrates the sensitivity of the optical spectra to the fitting parameters, namely the RMS roughness δ (Fig. 4(a) and (c)) and the relaxation rate factor for the Drude term α (Fig.4(b)). We see that the roughness parameter mostly affects plasmon resonance strength and does not affect absorption in the wavelength range between the resonances. The TE polarization spectra are not sensitive to changes in the roughness. The loss factor adjustment can be performed using off-resonance wavelengths since these spectral ranges are insensitive to the roughness. The spectra for the TE polarization provide appropriate sensitivity for the Lorentz factor adjustment (Fig.4(d)). All the parameters found from matching the experimental and simulated spectra are shown in Table 1.

Figure 5 collects the spectra of the imaginary part of the Ag dielectric function $\varepsilon_m''(\lambda, \alpha, \beta)$ for all five samples and both TM and TE polarizations. Corresponding changes in the real part of the dielectric function are negligible in accord with formula (4). The data for the bulk dielectric function from two literature sources [12-13] are shown for comparison. It should be noted that our results includes the size effect which results in an increased ε_m''. Figure 5a shows that as the strips width increases, the ε_m'' approaches the bulk value measured for a 34 nm film in [12]. The size dependence of the dielectric function is clearly seen here for both polarizations. We extracted the size-dependent term of the relaxation rate, $\gamma_{\text{size}} = \gamma(w) - \gamma_\infty = A V_F / w$, which is presented in Fig. 6(a) as a function of the inverse

#90392 - $15.00 USD Received 3 Dec 2007; revised 10 Jan 2008; accepted 11 Jan 2008; published 16 Jan 2008

effective width of the strips, $w_{eff}^{-1} = 0.5(w_t^{-1} + w_b^{-1})$. The simulations with two widths, representing the top and bottom strips, and simulations with the dielectric function using an effective width for both strips show good correspondence. The calculated A-parameters for the two polarizations are $A_{\mathrm{TM}} \approx 4.2 \pm 0.3$ and $A_{\mathrm{TE}} \approx 2.3 \pm 0.3$.

Table 1. Parameters of the samples.

Sample Parameters	Units	Sample #				
		1	2	3	4	5
width bottom-top	nm	174-94	160-85	164-72	127-39	118-20
thicknesses, Ag (Al_2O_3)	nm	30 (40)	35 (40)	35 (40)	35 (40)	35 (40)
period	nm	300	300	300	245	218
magnetic resonance wavelength	nm	791	727	720	588	536
electric resonance wavelength	nm	520	516	513	458	441
roughness (RMS)	nm	2.9	1.7	2.3	2.3	2.3
effective width $w_{eff} = 2/(w_t^{-1} + w_b^{-1})$	nm	122	111	100	60	34
relaxation rate factor, α (TE)		1.5±0.4	1.8±0.4	1.6±0.4	2.8±0.4	3.8±0.4
relaxation rate factor, α (TM)		3±0.4	3±0.4	2.8±0.4	4±0.4	7±0.4
Lorentz factor, $\beta \times \Gamma_{\mathrm{L}}$	eV	1.14	1.14	1.2×1.14	1.5×1.14	1.5×1.14

One can see that ε_m'' for the three samples with similar widths show almost no differences, indicating that the roughness does not affect the dielectric function. However, the distorting effect of roughness on the geometry is exhibited by the differences in the absorption spectra and the strong difference in the retrieved permeabilities of the effective layer, as is illustrated in Fig. 6(b).

The results of our experiments on the Ag dielectric function in coupled strips lead us to several important conclusions. First of all, the spectra of ε_m'' for the TE polarization (electric field parallel to the strips) suggest good quality of the Ag crystal structure. Indeed ε_m'' for

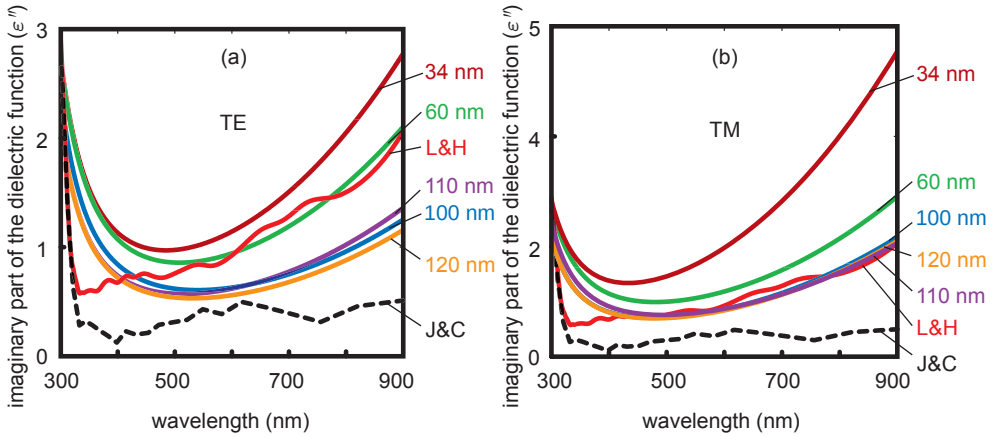

Fig. 5. The experimental spectra of the imaginary part of the Ag dielectric function in the coupled strips for five samples in comparison with the bulk dielectric function from two sources J&C, Ref. [12] and L&H, Ref. [13] for TE (a) and TM (b) polarizations.

#90392 - $15.00 USD Received 3 Dec 2007; revised 10 Jan 2008; accepted 11 Jan 2008; published 16 Jan 2008

samples with large widths are between the literature values from Johnson and Christy, and Lynch and Hunter [12-13] for bulk Ag carefully fabricated with subsequent polishing and annealing. As we mentioned above, a very probable reason for the diversity in the bulk Ag dielectric function is the term in the electron relaxation rate describing crystal defects and grain boundaries, ν_{ed}. The strips have a reasonable ε_m'' for the TE polarization, comparable with bulk, large-area films.

Surprisingly, roughness in the 1-6 nm range does not affect the Ag dielectric function. However, it strongly affects the plasmon coupling in paired strips and the resultant performance of the engineered material. We should mention that the achieved RMS roughness of about 1.7 nm is a very good result for the vacuum evaporation technique. Nevertheless, the tendency shown in Fig. 6(b) indicates a high potential for improvement of the negative permeability, provided that the surface roughness is on the order of atomic lattice scale.

A size-dependent increase of ε_m'' is detected for both polarizations. The A-parameter is larger for the TM polarization, which is indicative of a quantum size effect contribution that predicts anisotropy. The crystal defects could be also size-dependent. Chemical interface damping could be the reason for the size dependence at the TE polarization and anisotropy of the dielectric function.

According to Persson [7], an electron hits the particle surface, passes through the barrier, and occupies an adsorbate state. After some residence time, the electron may return to the particle. The tangential component of the internal current at the surface also contributes to $A_{\mathrm{interface}}$ via friction processes. These processes can be either elastic or inelastic, depending on the energy positions of the involved adsorbate levels relative to the Fermi energy. The energy transfer can be between zero and the whole "plasmon quantum energy." Moreover the tangential component provides a greater contribution to the $A_{\mathrm{interface}}$ than the normal component by factor 4-10 [9].

The chemical interface damping is proportional to the surface-to-volume ratio. Thus, one expects for TM polarization the tangential component to be proportional to the inverse thickness and the normal component proportional to be proportional to the inverse width of the strips, $\left(S/V\right)_{\mathrm{tangential}} \propto 1/t$, $\left(S/V\right)_{\mathrm{normal}} \propto 1/w$. For the TE polarization, one has only the tangential component, $\left(S/V\right)_{\mathrm{tangential}} \propto c_1/t + c_2/w$. Our results also show an abnormally large A-parameter for Ag strips relative to known A-parameters for spherical nanoparticles. The A-parameter is about 4.2 for the TM polarization calculated with an effective width, $w_{eff}^{-1} = 0.5\left(w_t^{-1} + w_b^{-1}\right)$.

The interface effect depends on particle shape in a way similar to that of the quantum size

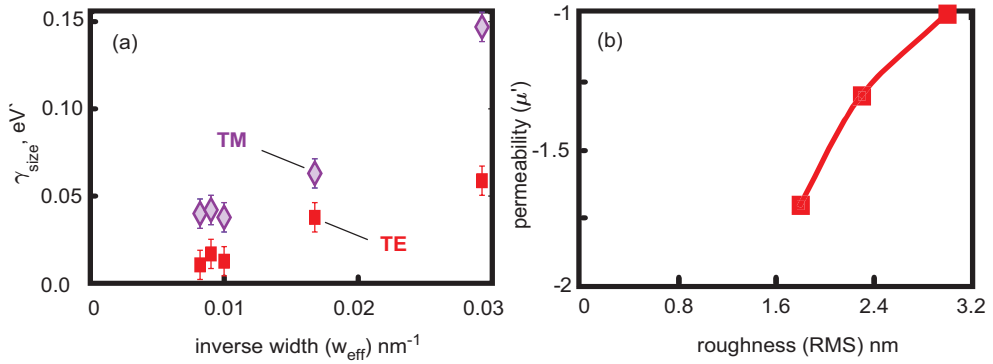

Fig. 6. (a) Size dependent term of the relaxation rate (eV) versus the inverse effective width of the strips for TM (blue squares) and TE (red circles) polarizations. (b) the real part of effective permeability vs. the RMS of surface roughness.

#90392 - $15.00 USD Received 3 Dec 2007; revised 10 Jan 2008; accepted 11 Jan 2008; published 16 Jan 2008

effect dependence. The theories presented in [5,7,9] deal with spherical particles. However one can estimate an expected value using an observation by Kraus and Schatz [15] that most of the shape dependence is the direct result of the shape dependence of the average length, $L_{av} = V/S$, defined as the ratio of the particle volume to the projected area of the particle perpendicular to the direction of the applied field. For the tangential component, it is expected that there should be a projected area of the particle parallel to the applied field. This shape factor, calculated for a spherical quantum well and rectangular quantum box, increases by about 1.5 for the rectangular prism [15]. Thus, taking the experimental value of $A = A_{\text{size}} + A_{\text{interface}} = 1.6$ for spheroidal particles [5] and multiplying by the factor 1.5, one might expect $A = 2.4$ for the rectangular prism. This rough estimate is still significantly less than our experimental values. On the other hand, the size-dependent contribution to the width for the rectangular prism with the field applied along the x axis is

$$\gamma_{\text{size}} = 1.5\, V_F / L_x \,. \tag{5}$$

The quantum mechanical treatment [15] predicts $A_{\text{size}} = 1.5$. In the case of spheroidal particles, the interface effect enhances the A-parameter by a factor of 6 [5]. This means that large values of the A-parameter are possible and likely due to the chemical interface effect.

It would be realistic to assume another damping channel caused by grain boundaries, especially in the case of TE polarization. Indeed, it is hard to expect that the strips along their long axis have properties of an ideal metal with a bulk relaxation constant.

4. Conclusions

To summarize, the Ag dielectric function for moderately sized (about 100 nm) strips differs from that of bulk Ag and is size-dependent for both polarizations of light. The measured transmission and reflection spectra of several samples are matched with those simulated by a frequency domain finite element method. Surface roughness was introduced in the modeling of the paired strips. Surprisingly, the geometrical effect of roughness is mostly responsible for increased losses at the plasmon resonances of the coupled particles, while the surface roughness does not affect the Ag permittivity. Anisotropy in ε_m'' observed in the experiments indicates a significant contribution from the quantum size effect and the chemical interface effect. The size-dependent terms of ε_m'' for two polarizations have relatively large A-parameters.

The spectra of ε_m'' for the TE polarization (electric field parallel to the strips) suggest good quality of the Ag crystal structure since the absolute values of ε_m'' for samples with large widths are between the literature values for bulk Ag, J&C [12] and L&H [13]. As we mentioned already the diversity in the imaginary part of the bulk dielectric function can be attributed to the electron collision rate with defects like crystal boundaries. In that sense the difference between different sources indicates a difference in the quality of silver films under test. Data from J&C and L&H show a range of typical quality Ag films, with better quality in the case of J&C. Note that size effects and volume defects can only increase the imaginary part of the dielectric function. Thus the results of this work on ε_m'' better match with Johnson&Christy data. Hence we conclude that the J&C paper provides more reliable data for a *good quality* bulk silver.

Acknowledgements

This work was supported in part by ARO grant W911NF-04-1-0350 and by ARO-MURI award 50342-PH-MUR.

#90392 - $15.00 USD Received 3 Dec 2007; revised 10 Jan 2008; accepted 11 Jan 2008; published 16 Jan 2008